Strain sensitive conductive polyurethane foam/graphene nanocomposites prepared by impregnation method (https://doi.org/10.1016/j.eurpolymj.2017.03.035)

Lorena Ugarte[1], Sandra Gómez-Fernández[1], Agnieszka Tercjak[1], Ana Martínez-Amesti[2], Maria Angeles Corcuera[1], Arantxa Eceiza[1],*

[1] "Materials + Technologies" Research Group (GMT), Department of Chemical and Environmental Engineering, Engineering College of Gipuzkoa, University of the Basque Country UPV/EHU, Plaza Europa 1, 20018 Donostia-San Sebastian, Spain

[2] Electronic Microscopy and Material Microanalysis, SGIker, Science and Technology Faculty, University of the Basque Country UPV/EHU, Barrio Sarriena s/n, 48940 Leioa, Spain.

Conductive polyurethane foam nanocomposites were prepared by the incorporation of graphene flakes. Graphene flakes were obtained from graphite by the top-down method of liquid exfoliation in N-methyl pyrrolidone and size-selected by centrifugation. A deep characterization of graphene flakes was performed for a better understanding of their role as nanoentities in polyurethane foam matrix. Thus, morphology, with special emphasis in the number of layers, was analyzed by Raman spectroscopy, atomic force microscopy and transmission electron microscopy. Electrostatic force microscopy was used to verify the conductive nature of graphene flakes. This technique showed to be effective for the assessment of both morphology and conductive properties of graphene flakes. Regarding the electrical behavior of the nanocomposite foams, it was determined that the electrical resistance depended on both the graphene content and the compressive deformation applied to the material.

Keywords: conductive polyurethane foam, nanocomposites, graphene, morphology, electrical properties.

1. Introduction

---

* Corresponding author. Tel: +0034 943017185. E-mail: arantxa.eceiza@ehu.eus

Graphene is a 2D material comprised of carbon atoms forming hexagonal lattices. Its characteristic structure confers graphene excellent electrical, thermal, mechanical and optical properties, becoming a material of great interest in the last years [1,2]. Common methods for graphene isolation include mechanical exfoliation, thermal decomposition of SiC, growth in nickel or copper substrates and graphene oxide exfoliation or liquid phase exfoliation of graphite [3]. Liquid phase exfoliation technique has shown great potential for the production of defect-free graphene flakes in large quantities due to the simplicity and profitability of the process [4–6]. In fact, liquid phase exfoliation process used in this work has demonstrated that graphene is fast and simply obtained by exfoliation in N-methyl pyrrolidone. In addition, the solvent can be recovered for further exfoliations, increasing the sustainability of the process.

The properties of graphene make it an interesting material for diverse applications in electronics [7], energy storage [8,9], electrochemistry [10], sensors [11–13], biomaterials and biomedicine [14–16] or food industry [17], among others. In the field of polymeric materials, graphene is an interesting material for polymer nanocomposites preparation with electrical [18], shape memory [19,20], or enhanced mechanical properties [21,22]. Conductive polyurethane foam nanocomposites are attracting attention in sensing applications due to their deformability and the sensitivity of electrical resistance to external loads. Recent works in this field include conductive polyurethane foams prepared with reduced graphene oxide by dip coating [23,24] or ultrasonication [25], as well as nanocomposites with graphene prepared by freeze drying [26] or water vapor induced phase separation [27]. For the preparation of nanocomposites, graphene in small flakes is preferred. However, it has been reported that graphene flake size plays an important role both in mechanical and electrical properties of the final material [21]. Several techniques have been used to characterize the morphology and electrical conductivity of grapheme such as optical microscopy [3], Raman spectroscopy [28,29], atomic force microscopy [30] or transmission electron microscopy [31,32]. Electrostatic force microscopy has been used to characterize the electrical properties of carbon materials such as carbon nanotubes [33,34].

In this work, ultrasound assisted impregnation method was used for the preparation of conductive nanocomposites, since it is a suitable, low cost and versatile method for the preparation of nanocomposites with carbonaceous nanoentities [35]. Considering the porous nature of polyurethane foam, sonication may favor the penetration of graphene into the matrix pores as well as the anchoring in the foam [25] as well as a more uniform dispersion of the graphene during the impregnation. The influence of graphene content and the compressive deformation applied to the material over the electrical resistance of the nanocomposites was analyzed. Graphene flakes were obtained from graphite by liquid exfoliation and centrifuged at different rates to obtain size-selected graphene

fractions. The morphology of graphene flakes was characterized by Raman spectroscopy, atomic force microscopy (AFM) and transmission electron microscopy (TEM). For the assessment of conductive properties electrostatic force microscopy (EFM) technique was used. Conductive polyurethane foam graphene nanocomposites were prepared by the ultrasound assisted impregnation method. The morphology and electrical properties of the nanocomposites were assessed by scanning electron microscopy (SEM) and Keithley equipment for the analysis of semiconductors.

2. Experimental Section

2.1. Materials and methods

Graphite flakes were purchased from Aldrich. N-methyl pyrrolidone (NMP) (Sigma-Aldrich) was used for the exfoliation process.

Polyurethane foam matrix was synthesized with Lupranol® 3423 polyol (BASF), distilled water (1 pphp), Tegoamin® B75 amine catalyst (0.45 pphp) used as blowing catalyst, DBTDL (0.63 pphp) used as gelling catalyst, Tegostab® 8404 surfactant (3 pphp) (Evonik) and 1,6-hexamethylen diisocyanate (HDI) (Desmodur H, Covestro). Cyclohexane (CH) and tetrahydrofurane (THF) were purchased from Scharlau and Sigma-Aldrich, respectively.

2.1.1. Exfoliation and size selection of graphene

Graphite was sonicated in NMP (20 g/1.5 L) for 100 h in an ultrasonic bath. The obtained graphene dispersion was centrifuged at 4000 rpm for 45 min and the upper part of the supernatant (ca. 80%) was collected. The sediment was redispersed for 15 min in an ultrasonic bath after incorporating 50 mL of NMP. Centrifugation and redispersion steps were repeated for 3000, 2000, 1000 and 500 rpm centrifugation rates according to the procedure described in literature to obtain graphene fractions of different sizes [36]. The dispersions were then filtered through polyamide filters (Sartorius, 0.2 µm pore size) and NMP was collected for future exfoliations. The graphene on the filter was washed with acetone to remove possible solvent traces and vacuum dried at ambient temperature for 48 h.

Graphene fractions were designated as S1, S2, S3, S4 and S5 according to a final centrifugation rate of 4000, 3000, 2000, 1000 and 500 rpm, respectively.

98 *2.1.2. Synthesis of polyurethane foam*

99

100 Foams were synthesized according to the procedure reported previously [37]. In this case, an aliphatic

101 isocyanate was used to locate the glass transition temperature of the foam at around room temperature,

102 for possible shape memory applications. Briefly, all reactants except HDI were mixed at 2000 rpm for

103 2 min with a high-shear stirrer. Then, HDI was added and mixing continued for 4 min. The used

104 isocyanate index used was 105. The reactive mixture was poured to an open mold and was left to rise

105 freely. Foam was cured for 24 h at room temperature before demolding.

106

107 *2.1.3. Preparation of polyurethane foam/graphene nanocomposites*

108

109 For the preparation of nanocomposites, a dispersion of S1 graphene in cyclohexane was prepared

110 (1 mg mL^{-1}), and bath sonicated for 30 min. Two foams were immersed in the graphene suspension

111 and bath sonicated for 15 and 10 min, respectively. To evaporate the solvent, the nanocomposites

112 were maintained at 35 °C for 15 h, at 500 mbar. Nanocomposites were designed as FG1 and FG2

113 according to a sonication time of 15 and 10 min, respectively. The graphene content of each

114 nanocomposite was determined by thermogravimetric analysis performed under N_2 atmosphere at a

115 scan rate of 10 °C min^{-1} (TGA/SDTA 851 Mettler Toledo), obtaining values of 3.3 and 2.8 wt% for

116 sample FG1 and FG2, respectively, from the residue analysis.

117

118 **2.2. Characterization techniques**

119

120 *2.2.1. Raman spectroscopy*

121

122 Raman spectra of graphene flakes were obtained with a Renishaw InVia microscope (50X) with a

123 laser of 514 nm wavelength (Modu Laser) at a potency of 10%. Data were collected in the range

124 of 150-3500 cm^{-1}. Exposure time and accumulations were set at 20 s and 5, respectively.

125

126 *2.2.2. Atomic force microscopy*

127

128 Atomic force microscopy (AFM) analysis was carried out to observe the size of graphene flakes.

129 Height images were obtained in a Dimension Icon scanning probe microscope equipped with

130 Nanoscope V controller (Bruker). Tapping mode was employed in air using an integrated

131 tip/cantilever (125 µm length with ca. 300 kHz resonant frequency).

132 For sample preparation, S1, S3, S4 and S5 fractions were dispersed in cyclohexane (CH) (0.005

133 mg mL^{-1} for S1 and S3 and 0.0025 mg mL^{-1} for S4 and S5) using an ultrasonic tip for 1 h. The

134 selection of the solvent was done according to one possible application of graphene flakes in

135 polyurethane foam nanocomposites preparation. To avoid solvent evaporation, a pulsed sonication

136 program was applied, with ON/OFF periods of 4 and 2 s, respectively. A droplet of graphene

137 suspension was put on a prewashed silicon wafer substrate and dried at room temperature for

138 48 h.

139

140 *2.2.3. Transmission electron microscopy*

141

142 Transmission electron microscopy (TEM) was used to assess the morphology of graphene and

143 determination of the number of layers. Measurements were carried out on a FEI Titan Cubed G2 60-

144 300 microscope, equipped with a Schottky X-FEG field emission electron gun, monochromator and

145 CEOS GmbH spherical aberration (Cs) corrector on the image side. The microscope was operated at

146 80 kV to minimize the knock-on damage to the graphene. The third-order spherical aberration (C_s)

147 was tuned to -10 µm. Images were obtained for an underfocus of -8 nm and were recorded on a CCD

148 camera (2kx2k, Gatan UltraScan 1000), using exposition times of 1s per image.

149 For sample preparation, graphene flakes were dispersed in tetrahydrofuran (THF) at 0.005 mg mL^{-1}

150 for 1h, using an ultrasonic tip. To avoid excessive heating, pulsed sonication program was applied,

151 with ON/OFF periods of 4 and 2 s, respectively. A drop of suspension was spread onto a TEM copper

152 grid (300 Mesh) covered by a holey carbon film followed by drying under vacuum.

153

154 *2.2.4. Electrostatic force microscopy*

155

156 Electrostatic force microscopy (EFM) measurements were carried out in the same Dimension Icon

157 scanning probe microscope operating in the lift mode (100 nm) in ambient conditions and

158 equipped with a Pt/Ir coated tip (ca. 75 kHz resonant frequency). The same samples employed

159 for AFM analysis were used. The secondary imaging mode derived from the tapping mode that

160 measures the electric field gradient distribution above the sample surface was detected by applying

161 a 6 V voltage to the cantilever tip.

162

163 2.2.5. Scanning electron microscopy

164

Scanning electron microscopy (SEM) images of nanocomposites were obtained in a JEOL JSM-6400 equipment with 20 kV acceleration voltage and using electron beam currents of 0.05-0.1 nA. Prior to analysis, samples were gold coated (20 nm).

169 2.2.6. Electrical properties

Electrical properties of nanocomposites were analyzed by a Keithley 4200-SCS equipment for semiconductors analysis. Two point measurements were carried out, performing 0-5 V linear scans, with 0.01 V step and a compliance of 0.1 A. Electrical resistance (R) values were calculated from intensity vs. voltage curves. To perform the measurements, a home-built dispositive was used. Nanocomposites were placed in contact with two copper sheets, adhered in turn to polycarbonate plates. To close the electric circuit two copper wires, which came up from the copper plates, were put in contact with the electrodes of the equipment. To measure the changes of electrical resistance as a consequence of compressive deformation, the polycarbonate plates were placed in a clamp to apply a controlled deformation to the sample. The distance between polycarbonate plates was verified with a caliper before each measurement. The dimensions of the nanocomposites were 10 x 10 mm^2 section and 20 mm height.

3. Results and Discussion

3.1. Raman spectroscopy

Results regarding Raman spectroscopy were summarized in Figure 1. Raman spectra of graphene samples are shown in Figure 1a. All spectra present typical bands associated with carbon materials: G band (1580 cm^{-1}), 2D band (2700 cm^{-1}) and D band (1350 cm^{-1}). G band is associated with an in-plane vibration mode due to the bond stretching of sp^2 carbon pairs and 2D band is related to the second order of zone boundary phonons [4,38]. D band needs a defect for its activation and it is associated with flake edges [29,28]. Differences of graphite and graphene spectra may confirm the effective exfoliation of graphite. Changes in shape and intensity of 2D band were observed when compared graphene to graphite [38,28]. Moreover, the D peak intensity was very small in graphite while it increased in graphene samples. The I_D/I_G ratio is a good indicator of the in-plane crystallite size since is related with new edges formed as the average flake size is reduced by sonication [5,29,39]. The I_D/I_G ratio with relation to centrifugation rate is shown in Figure 1b. According to the

previously mentioned, the creation of new edges when compared to graphite powder suggested a decrease of flake size with the increase in final centrifugation rate.
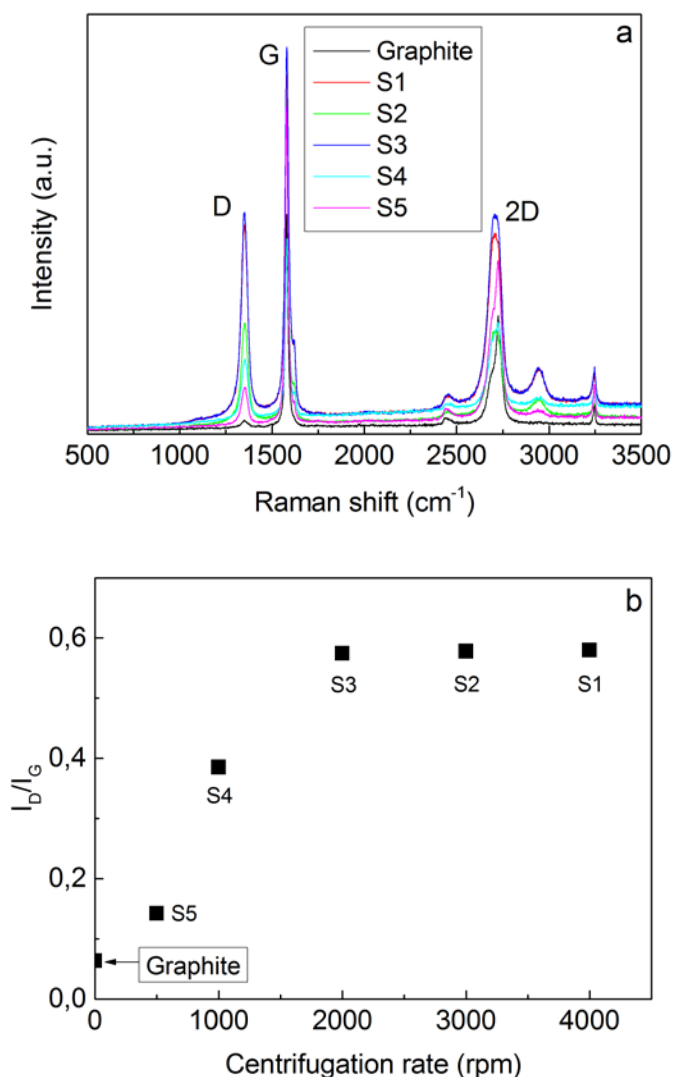

Figure 1. Raman spectra (a) and I_D/I_G ratio (b) of exfoliated graphene fractions and graphite.

3.2. Atomic force microscopy

Flake size was analyzed by AFM and related with Raman I_D/I_G ratio. Sample S2 was not analyzed since it had very similar I_D/I_G ratio to S1 and S3 fractions. AFM height images and their corresponding cross sectional height profiles are shown in Figure 2. A gradual decrease of flake size is observed with the increase of final centrifugation rate. Flake sizes of around 5 µm were observed in Figure 2a and Figure 2b corresponding to S5 and S4 fractions, respectively. An evident decrease of flake size was observed in the fractions centrifuged at higher rates, with values of ca. 400-500 nm (Figure 2c and 2d). Results were quite in agreement with Raman analysis. AFM height

210 images revealed the formation of agglomerates in S4 and S5 fractions, suggesting the presence of

211 poorly exfoliated bulk graphite due to the low centrifugation rate, especially in S5 fraction, which

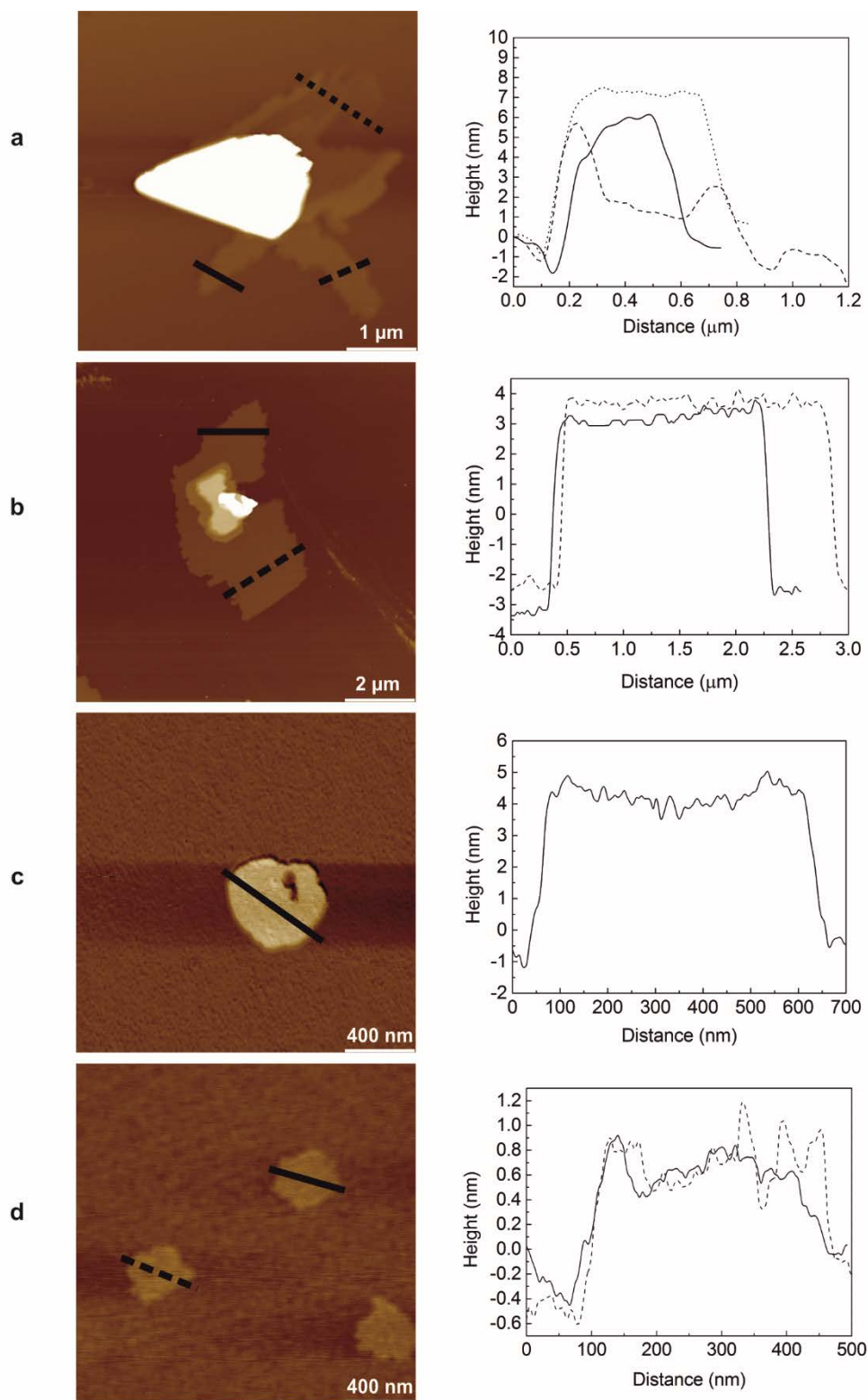212 could also be responsible for its low I_D/I_G ratio.

Figure 2. AFM height images (left) and cross sectional profiles (right) of (a) S5, (b) S4, (c) S3 and

(d) S1 graphene fractions.

213 The determination of the number of layers by AFM depends on the substrate as well as on the
214 tip-sample interactions [40]. Number of layers (*N*) could be estimated according to Equation 1 [30]:

215

$$N = \frac{t_{AFM} - 0.4}{0.335}$$ (Eq. 1)

216

217 where t_{AFM} is the thickness measured by AFM, *0.4* is a factor to take into account substrate-
218 graphene and graphene-tip interactions and *0.335* corresponds to graphite inter-plane spacing (0.335
219 nm). According to cross sectional profiles of S1 fraction, graphene flakes had an approximated
220 thickness of 1.5 nm, which may correspond to few layer graphene. Thickness of S3 graphene
221 was in the range of 4-5 nm, corresponding to multilayer graphene. Thickness values of 6 and 8 nm
222 were calculated from S4 and S5 graphene, respectively. Reported flake size and thickness values
223 were in the range of those reported in literature [36,41]. A decrease of graphene thickness and
224 flake size was observed with the increase of final centrifugation rate, indicating that smaller but
225 better exfoliated few layer graphene flakes were separated at high centrifugation rates. Visual
226 evaluation of the dispersions, shown in Figure 3, also suggested bigger flake sizes for S4 and S5
227 dispersions due to the higher turbidity observed. For comparative purposes, all dispersions were
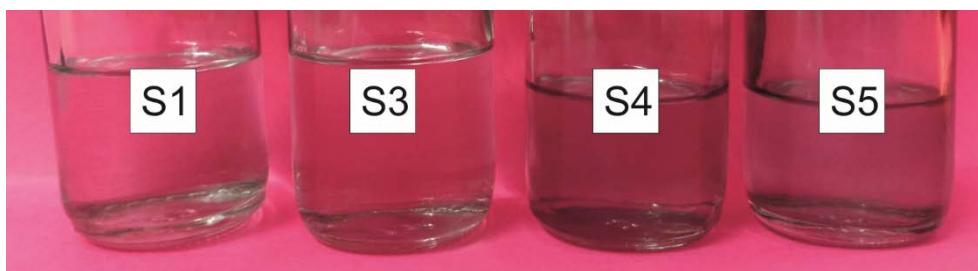228 prepared at the same concentration of 0.005 mg mL^{-1}.

Figure 3. S1, S3, S4 and S5 dispersions prepared at 0.005 mg mL^{-1} in CH

229

230 **3.3. Transmission electron microscopy**

231

232 According to AFM results, S1 fraction consisted of few layer graphene flakes. To perform a deeper
233 analysis of the number of layers in S1 graphene, the sample was analyzed by TEM. Figure 4 shows a
234 low magnification TEM image of the analyzed flake on the grid carbon layer. The analysis of the
235 areas on the flake indicated as "1" and "2" on Figure 4, made possible to assess the number of layers.
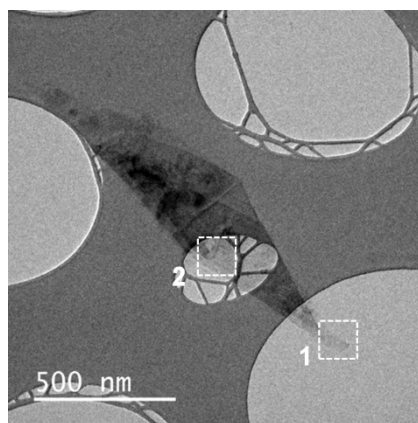
Figure 4. TEM image of analyzed S1 graphene flake.

236

237 Figure 5 left images show the magnifications performed on "1" area (Figure 5a and 5b) and the

238 magnification performed on "2" area (Figure 5c). Figure 5 center images show the magnifications of

239 the areas delimited by the dashed rectangles on the left images. On the same fashion, Figure 5 right

240 images show the magnifications of the areas delimited by the dashed rectangles on the center images.

241 Regarding images on the center and right, carbon structures could be distinguished in the three areas,

242 each area showing different patterns. Each pattern might be indicative of the number of layers [42].

243 Basing on Warner et al. work [42], the patterns observed in Figure 5 (right) were related with the

244 number of layers. According to this, the triangular pattern observed in Figure 5a should be

245 characteristic of 3 or 5 layer graphene. In Figure 5b a hexagonal pattern could be distinguished, where

246 carbon atoms showed bright contrast. This pattern is observed in graphene of even numbers of layers

247 and also in graphene of 7-9 layers. However, it was not possible to relate these patterns with a specific
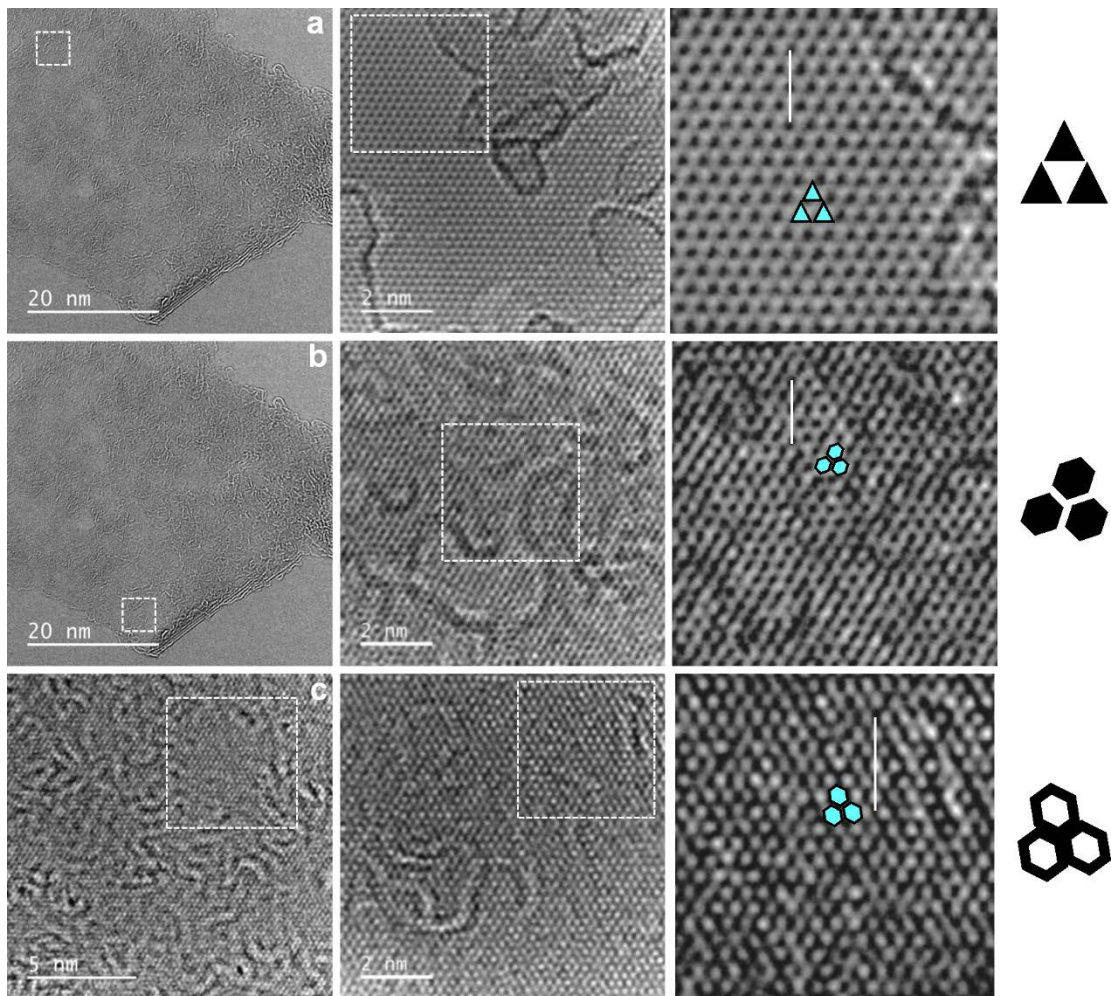
248 number of layers.

Figure 5. TEM images (a and b) taken from zone 1 and (c) taken from zone 2 defined in previous figure (left), TEM images obtained from the areas indicated by the dashed rectangles on the left (center) and TEM images obtained from the areas indicated by the dashed rectangles on the center (right).

249 Figure 5c also showed a hexagonal pattern where the carbon atoms showed dark contrast. Carbon
250 atoms in monolayer graphene show dark contrast when working under focus [34], as in this case.
251 Apart from pattern analysis, the intensity line profiles (calculated along the white lines in Figure 5,
252 right) were plotted in order to quantify the number of layers [42] (Figure 6).
253 On the profiles shown in Figure 6a and Figure 6b a split in the main peak is observed, which means
254 that two carbon atoms column is asymmetric. The asymmetry was determined following the method
255 of Warner et al. [42] The as obtained ratio values were 1.69, 1.57 and 1.74 for Figure 6a and 1.1, 1.3
256 and 1.03 for Figure 6b. Basing on these results, it could be supposed that the area analyzed in Figure
257 6a consists of 5 layer graphene and the area analyzed in Figure 6b consists of 9 layer graphene.
258 Finally, the profile on Figure 6c showed a dip in the line profile, which means that this area is
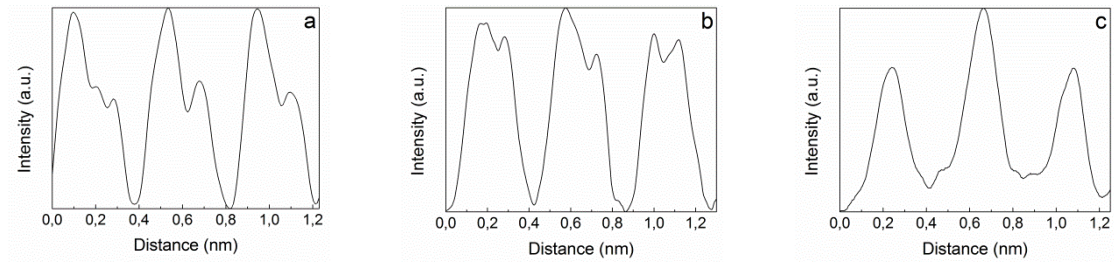
259   composed by monolayer graphene.

Figure 6. Intensity profiles calculated along the white lines shown in (a) Figure 5a right, (b) Figure
5b right, and (c) Figure 5c right.

260

261   **3.4. Electrostatic force microscopy**

262

263   EFM analysis was used to prove the conductive properties of few layer S1 graphene flakes. In
264   EFM analysis, an electrostatic field is created between the tip and the substrate. When the sample is
265   scanned at a sufficient height (100-200 nm) to avoid van der Waals interactions, the deflection of
266   the cantilever is influenced by the electrostatic forces created between the tip and the substrate [43].
267   To perform EFM measurements, two pass scans are performed. On the first scan, topographical
268   information of the sample is collected in tapping mode AFM. On the second scan, the tip is lifted
269   to a predetermined height so as the interactions only depend on electric properties. A direct current
270   voltage is applied to the tip and the scan is performed maintaining a constant tip-sample separation
271   based on topographical data. Analyzing phase shifts on the cantilever allows distinguishing between
272   insulating and conductive parts of the sample [34,33].
273   EFM characterization of S1 graphene fraction is shown in Figure 7. There is no response observed
274   when 0 V voltage is applied to the sample, indicating that results are not influenced by the
275   topography of the sample and the applied lift height is correct, as previously mentioned. Graphene
276   flakes can be distinguished when a voltage is applied to the tip. In the case of -6 V applied voltage
277   a dark contrast is observed on the phase image indicating attractive forces between the tip and the
278   sample. On the contrary, when 6 V voltage is applied, graphene flakes appear bright indicating
279   repulsive forces between the tip and the sample. This behavior is typical of positively charged
280   specimens, where Coulomb interactions are dominant over induced polarization effects [44,45].
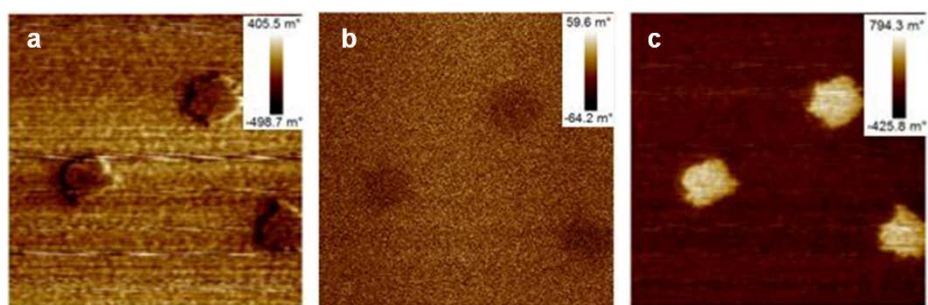
Figure 7. EFM phase images obtained at bias voltage of -6 V (left), 0V (center) and 6 V (right) of S1 graphene fraction. Scan size: 2 µm x 2 µm

3.5. Cellular structure of polyurethane foam/graphene nanocomposites

The cellular structure of the foam matrix and nanocomposites was analyzed by SEM and the obtained images are shown in Figure 8. When comparing nanocomposites with bare foam matrix, it could be seen that some cell walls were torn possibly due to the sonication technique used for the incorporation of graphene. Moreover, in the images obtained at 50X magnification some particles which could be stacked graphene flakes were observed. Analyzing the cell walls at higher magnification (10000X) some flakes which could correspond to graphene were observed. Their appearance was in accordance to other structures observed in some works concerning polymer/graphene nanocomposites [46–48].
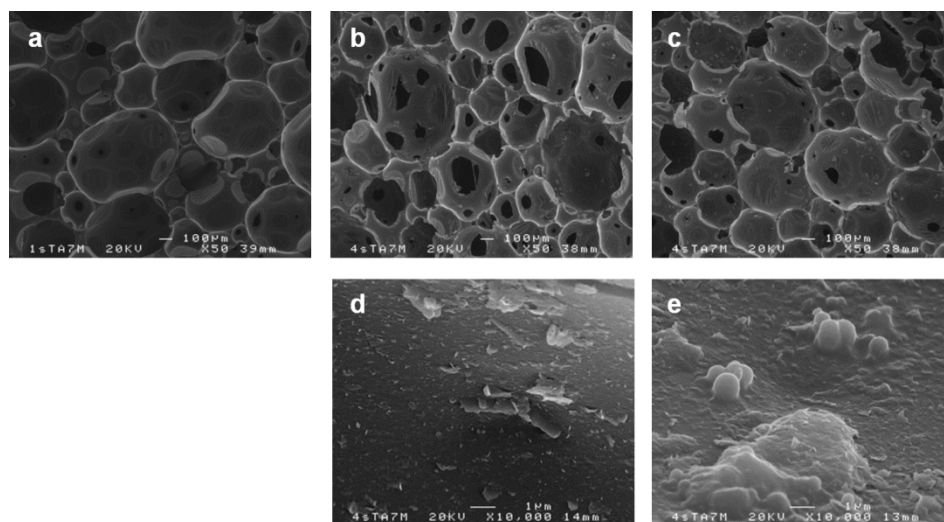
Figure 8. SEM images of (a) foam matrix, (b) FG1 and (c) FG2 nanocomposites obtained at 50X magnification and SEM images of (d) FG1 and (e) FG2 nanocomposites obtained at 10000X magnification.

3.6. Electrical properties of nanocomposites

The electrical properties of the nanocomposites were analyzed from intensity-voltage curves, obtained in Keithley equipment for the analysis of semiconductors. Undeformed nanocomposites, Figure 9a, showed a linear intensity-voltage relationship and the curve corresponding to each nanocomposite showed different slopes, suggesting that the electrical resistance of each one would be different. The electrical resistance values, calculated by applying the Ohm's law, were of 0.3×10^6 and 5.0×10^6 Ω for samples FG1 and FG2, respectively. According to this, semiconductor nanocomposites were obtained by the incorporation of low contents of graphene [49]. Moreover, it was observed that graphene content had a direct effect over the electrical resistance of the nanocomposites.

Apart from the adhered graphene content, the differences of the electrical resistance as a consequence of compressive deformation were analyzed. Each nanocomposite was compressed until a 70% deformation value and the change in electrical resistance for each deformation value was measured (Figure 9b). A reduction on the electrical resistance was observed when the sample was deformed. Regions of different behavior were observed in the curves. At very low deformations (until 5-6%) the decrease of the electrical resistance was pronounced. In intermediate deformations nanocomposites showed a plateau-like behavior. At high deformations (above 40%) the decrease of the electrical resistance was again notorious. It was observed that these three regions would coincide with compressive stress-strain curves of polyurethane foams [50]. According to this, the first region would correspond to the elastic bending of foam cell struts. In the plateau region cell struts are supposed to collapse and consequently deformation values increase with low changes in stress. In the last region, the cells would be collapsed and the stress increases rapidly with low deformations. Turning to the electrical properties, it seemed that the elastic bending of cell struts and the deformation posterior to cell collapse improves the contact between graphene flakes reducing the electrical resistance. The collapsing stage seemed not to have influence over this effect.
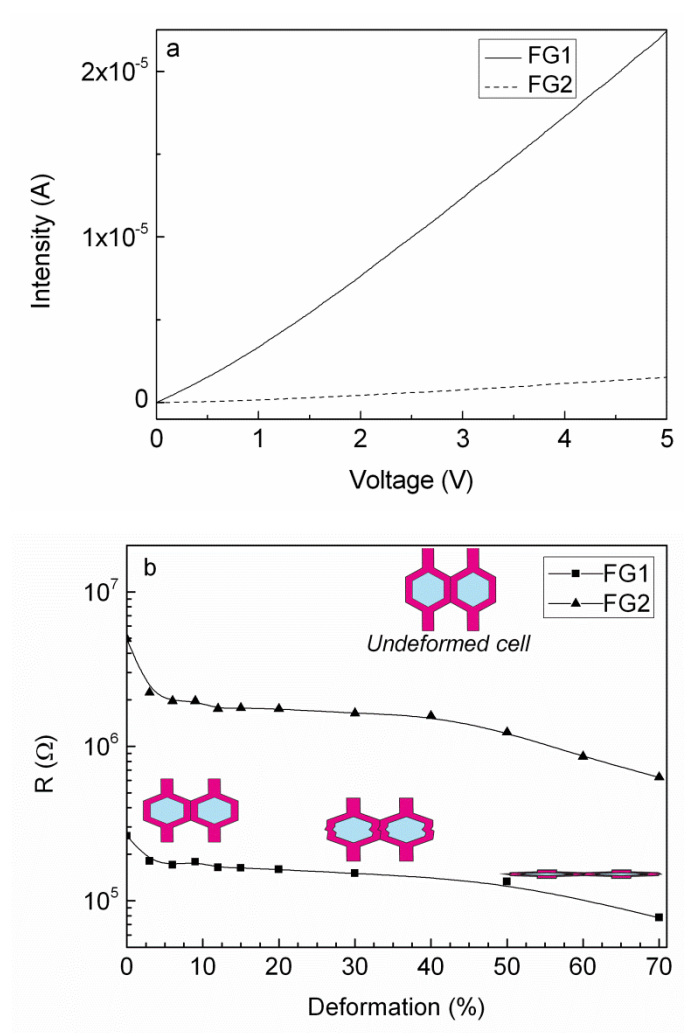
Figure 9. (a) Intensity-voltage curves of nanocomposites and (b) evolution of the electrical resistance of nanocomposites with the deformation.

4. Conclusions

Graphene flakes were obtained from graphite powder by liquid exfoliation technique using N-methyl pyrrolidone as solvent. The posterior separation by centrifugation proved to be suitable to obtain graphene fractions of different flake size depending on final centrifugation rate. Combination of Raman spectroscopy, atomic force microscopy and transmission electron microscopy allows to assess graphene flake size and the number of layers quantitatively. According to AFM analysis, flake size varied from 5 µm to 400 nm and flake thickness varied from 8 to 1.5 nm when final centrifugation rate changed from 500 to 4000 rpm, respectively. The reduced number of layers of S1 fraction was confirmed by TEM analysis. By means of electrostatic force microscopy both flake size and electrical conductivity could be assessed simultaneously and in a straightforward

manner.

Graphene containing polyurethane foam nanocomposites were successfully prepared by incorporating graphene flakes from S1 fraction to polyurethane foams by using the ultrasound assisted impregnation method. The presence of graphene flakes was checked by SEM analysis.

Graphene provides foam matrix with electrical conductivity. Graphene content has high influence of electrical resistance values. Apart from this, it was seen that the electrical resistance of the nanocomposites was sensitive to compressive mechanical deformation. This property confers the material potential applicability in sensing applications such as piezoresistive or pressure sensitive materials. The contact between graphene flakes seems to improve as a consequence of the elastic bending of cell struts and the structure posterior to cell collapse, diminishing the electrical resistance.

References

[1]   K.S. Novoselov, Nobel Lecture: graphene: materials in the flatland, Rev. Mod. Phys. 83 (2011) 837–849. doi:10.1103/RevModPhys.83.837.

[2]   K.S. Novoselov, V.I. Fal, L. Colombo, P.R. Gellert, M.G. Schwab, K. Kim, A roadmap for graphene, Nature. 490 (2012) 192–200. doi:10.1038/nature11458.

[3]   D.R. Cooper, B. D'Anjou, N. Ghattamaneni, B. Harack, M. Hilke, A. Horth, N. Majlis, M. Massicotte, L. Vandsburger, E. Whiteway, V. Yu, Experimental review of graphene, ISRN Condens. Matter Phys. 2012 (2012) 1–56. doi:10.5402/2012/501686.

[4]   S. Gayathri, P. Jayabal, M. Kottaisamy, V. Ramakrishnan, Synthesis of few layer graphene by direct exfoliation of graphite and a Raman spectroscopic study, AIP Adv. 4 (2014) 0–12. doi:10.1063/1.4866595.

[5]   U. Khan, A. O'Neill, M. Lotya, S. De, J.N. Coleman, High-concentration solvent exfoliation of graphene, Small. 6 (2010) 864–871. doi:10.1002/smll.200902066.

[6]   C. Soldano, A. Mahmood, E. Dujardin, Production, properties and potential of graphene,

369   Carbon N. Y. 48 (2010) 2127–2150. doi:10.1016/j.carbon.2010.01.058.

370 [7] W. Hua-Qiang, L. Chang-Yang, L. Hong-Ming, Q. He, Graphene applications in electronic

371   and optoelectronic devices and circuits, Chinese Phys. B. 22 (2013) 098106 (1-10).

372   doi:10.1088/1674-1056/22/9/098106.

373 [8] X. Fan, X. Chen, L. Dai, 3D graphene based materials for energy storage, Curr. Opin.

374   Colloid Interface Sci. 20 (2015) 429–438. doi:10.1016/j.cocis.2015.11.005.

375 [9] C. Chien, P. Hiralal, D. Wang, I. Huang, C. Chen, C. Chen, G.A.J. Amaratunga, Graphene-

376   based integrated photovoltaic energy harvesting/storage device, Small. 11 (2015) 2929–2937.

377   doi:10.1002/smll.201403383.

378 [10] H. Liu, J. Gao, M. Xue, N. Zhu, M. Zhang, T. Cao, Processing of graphene for

379   electrochemical application: noncovalently functionalize graphene sheets with water-soluble

380   electroactive methylene green, Langmuir. 25 (2009) 12006–12010. doi:10.1021/la9029613.

381 [11] V. Borislav, G. Rados, Graphene-covered photonic structures for optical chemical sensing,

382   Phys. Rev. Appl. 4 (2015) 024007 (1-11). doi:10.1103/PhysRevApplied.4.024007.

383 [12] S. Rumyantsev, G. Liu, M.S. Shur, R.A. Potyrailo, A.A. Balandin, Selective gas sensing with

384   a single pristine graphene transistor, Nano Lett. 12 (2012) 2294–2298.

385 [13] X. Dong, Y. Shi, W. Huang, P. Chen, L. Li, Electrical detection of DNA hybridization with

386   single-base specificity using transistors based on CVD-grown graphene sheets, Adv. Mater.

387   22 (2010) 1649–1653. doi:10.1002/adma.200903645.

388 [14] C. Fisher, A.E. Rider, Z.J. Han, S. Kumar, I. Levchenko, K.K. Ostrikov, Applications and

389   nanotoxicity of carbon nanotubes and graphene in biomedicine, J. Nanomater. 2012 (2012)

390   315185 (1-19). doi:10.1155/2012/315185.

391 [15] P. Zuo, H. Feng, Z. Xu, L. Zhang, Y. Zhang, W. Xia, W. Zhang, Fabrication of

392   biocompatible and mechanically reinforced graphene oxide-chitosan nanocomposite films,

393   Chem. Cent. J. 7 (2013) 1–11.

394 [16] M. Skoda, I. Dudek, A. Jarosz, D. Szukiewicz, Graphene: one material, many possibilities-

395   application difficulties in biological systems, J. Nanomater. 2014 (2014) 890246 (1-11).

396 [17] A.K. Sundramoorthy, S. Gunasekaran, Applications of graphene in quality assurance and

397   safety of food, Trends Anal. Chem. 60 (2014) 36–53. doi:10.1016/j.trac.2014.04.015.

398 [18] R.M. Hodlur, M.K. Rabinal, Self assembled graphene layers on polyurethane foam as a

399   highly pressure sensitive conducting composite, Compos. Sci. Technol. 90 (2014) 160–165.

400   doi:10.1016/j.compscitech.2013.11.005.

401 [19] S.M. Kang, S.J. Lee, B.K. Kim, Shape memory polyurethane foams, eXPRESS Polym. Lett.

402   6 (2012) 63–69. doi:10.3144/expresspolymlett.2012.7.

403 [20] H.Y. Huang, T.C. Huang, J.C. Lin, J.H. Chang, Y.T. Lee, J.M. Yeh, Advanced
404 environmentally friendly coatings prepared from amine-capped aniline trimer-based
405 waterborne electroactive polyurethane, Mater. Chem. Phys. 137 (2013) 772–780.
406 doi:10.1016/j.matchemphys.2012.09.063.

407 [21] P. May, U. Khan, A. O'Neill, J.N. Coleman, Approaching the theoretical limit for reinforcing
408 polymers with graphene, J. Mater. Chem. 22 (2012) 1278–1282. doi:10.1039/c1jm15467b.

409 [22] K. Nawaz, M. Ayub, N. Ul-Haq, M.B. Khan, M.B.K. Niazi, A. Hussain, Effects of selected
410 size of graphene nanosheets on the mechanical properties of polyacrylonitrile polymer,
411 Fibers Polym. 15 (2014) 2040–2044. doi:10.1007/s12221-014-2040-8.

412 [23] B. Shen, Y. Li, W. Zhai, W. Zheng, Compressible graphene-coated polymer foams with
413 ultralow density for adjustable electromagnetic interference (EMI) shielding, ACS Appl.
414 Mater. Interfaces. 8 (2016) 8050–8057. doi:10.1021/acsami.5b11715.

415 [24] H.-B. Yao, J. Ge, C.-F. Wang, X. Wang, W. Hu, Z.-J. Zheng, Y. Ni, S.-H. Yu, A flexible and
416 highly pressure-sensitive graphene-polyurethane sponge based on fractured microstructure
417 design, Advanced. 25 (2013) 6692–6698. doi:10.1002/adma.201303041.

418 [25] H. Shi, D. Shi, L. Yin, Z. Yang, S. Luan, J. Gao, J. Zha, J. Yin, R.K.Y.- Li, Ultrasonication
419 assisted preparation of carbonaceous nanoparticles modified polyurethane foam with good
420 conductivity and high oil absorption properties, Nanoscale. 6 (2014) 13748–13753.
421 doi:10.1039/c4nr04360j.

422 [26] H. Liu, M. Dong, W. Huang, J. Gao, K. Dai, J. Guo, G. Zheng, C. Liu, C. Shen, Z. Guo,
423 Lightweigh conductive graphene/thermoplastic polyurethane foams with ultrahigh
424 compressibility for piezoresistive sensing, J. Mater. Chem. C. 5 (2017) 77–83.
425 doi:10.1039/c6tc03713e.

426 [27] Y. Chen, Y. Li, D. Xu, W. Zhai, Fabrication of stretchable, flexible conductive thermoplastic
427 polyurethane/graphene composites via foaming, RSC Adv. 5 (2015) 82034–82041.
428 doi:10.1039/C5RA12515D.

429 [28] A.C. Ferrari, J.C. Meyer, V. Scardaci, C. Casiraghi, M. Lazzeri, F. Mauri, S. Piscanec, D.
430 Jiang, K.S. Novoselov, S. Roth, A.K. Geim, Raman spectrum of graphene and graphene
431 layers, Phys. Rev. Lett. 97 (2006) 1–4. doi:10.1103/PhysRevLett.97.187401.

432 [29] M.S. Dresselhaus, A. Jorio, R. Saito, Characterizing graphene, graphite, and carbon
433 nanotubes by Raman spectroscopy, Annu. Rev. Condens. Matter Phys. 1 (2010) 89–108.
434 doi:10.1146/annurev-conmatphys-070909-103919.

435 [30] C.J. Shearer, A.D. Slattery, A.J. Stapleton, J.G. Shapter, C.T. Gibson, Accurate thickness
436 measurement of graphene, Nanotechnology. 27 (2016) 125704 (1-10). doi:10.1088/0957-

437   4484/27/12/125704.

438   [31]   A. Bachmatiuk, J. Zhao, S.M. Gorantla, G.I. Gonzalez Martinez, J. Wiedermann, C. Lee, J.

439   Eckert, M.H. Rummeli, Low voltage transmission electron microscopy of graphene, Small.

440   11 (2015) 515–542. doi:10.1002/smll.201401804.

441   [32]   S. Akhtar, Transmission electron microscopy of graphene and hydrated biomaterial

442   nanostructures: novel techniques and analysis, Uppsala University, 2012.

443   [33]   L. Peponi, A. Tercjak, J. Gutierrez, M. Cardinali, M. Kenny, L. Valentini, I. Civile, Mapping

444   of carbon nanotubes in the polystyrene domains of a polystyrene-b-polyisoprene-b-

445   polystyrene block copolymer matrix using electrostatic force microscopy, Carbon N. Y. 8

446   (2010) 2590–2595. doi:10.1016/j.carbon.2010.03.062.

447   [34]   A. Bachtold, M.S. Fuhrer, S. Plyasunov, M. Forero, E.H. Anderson, A. Zettl, P.L. Mceuen,

448   Scanned probe microscopy of electronic transport in carbon nanotubes, Phys. Rev. Lett. 84

449   (2000) 6082–6085.

450   [35]   Y. Gunko, I. Mondragon, B. Fernández-d'Arlas, A. Eceiza, Método de recubrimiento de

451   superficies poliméricas con un recubrimiento que contiene carbono y producto obtenido por

452   dicho método, 2013.

453   [36]   U. Khan, A. O'Neill, H. Porwal, P. May, K. Nawaz, J.N. Coleman, Size selection of

454   dispersed, exfoliated graphene flakes by controlled centrifugation, Carbon N. Y. 50 (2012)

455   470–475. doi:10.1016/j.carbon.2011.09.001.

456   [37]   L. Ugarte, S. Gómez-Fernández, C. Peña-Rodríguez, A. Prociak, M.A. Corcuera, A. Eceiza,

457   Tailoring mechanical properties of rigid polyurethane foams by sorbitol and corn derived

458   biopolyol mixtures, ACS Sustain. Chem. Eng. 3 (2015) 3382–3387.

459   doi:10.1021/acssuschemeng.5b01094.

460   [38]   A.C. Ferrari, Raman spectroscopy of graphene and graphite: Disorder, electron-phonon

461   coupling, doping and nonadiabatic effects, Solid State Commun. 143 (2007) 47–57.

462   doi:10.1016/j.ssc.2007.03.052.

463   [39]   A. O'Neill, U. Khan, P.N. Nirmalraj, J. Boland, J.N. Coleman, Graphene dispersion and

464   exfoliation in low boiling point solvents, J. Phys. Chem. C. 115 (2011) 5422–5428.

465   doi:10.1021/jp110942e.

466   [40]   F. Bonaccorso, A. Lombardo, T. Hasan, Z. Sun, L. Colombo, A.C. Ferrari, Production and

467   processing of graphene and 2d crystals, Mater. Today. 15 (2012) 564–589.

468   doi:10.1016/S1369-7021(13)70014-2.

469   [41]   L. Zhu, X. Zhao, Y. Li, X. Yu, C. Li, Q. Zhang, High-quality production of graphene by

470   liquid-phase exfoliation of expanded graphite, Mater. Chem. Phys. 137 (2013) 984–990.

471   doi:10.1016/j.matchemphys.2012.11.012.

472 [42]   J.H. Warner, The influence of the number of graphene layers on the atomic resolution images

473   obtained from aberration-corrected high resolution transmission electron microscopy,

474   Nanotechnology. 21 (2010) 255707 (1-5). doi:10.1088/0957-4484/21/25/255707.

475 [43]   H. Etxeberria, A. Tercjak, I. Mondragon, A. Eceiza, G. Kortaberria, Electrostatic force

476   microscopy measurements of CdSe-PS nanoparticles and CdSe-PS/poly (styrene-b-

477   butadiene-b-styrene) nanocomposites, Colloid Polym. Sci. 292 (2014) 229–234.

478   doi:10.1007/s00396-013-3061-3.

479 [44]   A. Gruverman, Nanoscale phenomena in ferroelectric thin films. Chapter III, Springer, New

480   York, 2004.

481 [45]   J. Kim, W.J. Jasper, J.P. Hinestroza, Charge characterization of an electrically charged fiber

482   via electrostatic force microscopy, J. Eng. Fiber. Fabr. 1 (2006) 30–46.

483 [46]   H. Devnani, S.P. Satsangee, R. Jain, A novel graphene-chitosan-Bi2 O3 nanocomposite

484   modified sensor for sensitive and selective electrochemical determination of a monoamine

485   neurotransmitter epinephrine, Ionics (Kiel). 22 (2016) 943–956. doi:10.1007/s11581-015-

486   1620-y.

487 [47]   D. Nuvoli, V. Alzari, R. Sanna, S. Scognamillo, J. Alongi, G. Malucelli, A. Mariani,

488   Synthesis and characterization of graphene-based nanocomposites with potential use for

489   biomedical applications, J. Nanoparticle Res. 15 (2013) 1512 (1-8). doi:10.1007/s11051-013-

490   1512-x.

491 [48]   S. Sahoo, P. Bhattacharya, G. Hatui, D. Ghosh, C.K. Das, Sonochemical synthesis and

492   characterization of amine-modified graphene/conducting polymer nanocomposites, J. Appl.

493   Polym. Sci. 128 (2013) 1476–1483. doi:10.1002/app.38285.

494 [49]   B. Fernández-d'Arlas, U. Khan, L. Rueda, J.N. Coleman, I. Mondragon, M.A. Corcuera, A.

495   Eceiza, Influence of hard segment content and nature on polyurethane/multiwalled carbon

496   nanotube composites, Compos. Sci. Technol. 71 (2011) 1030–1038.

497   doi:10.1016/j.compscitech.2011.02.006.

498 [50]   D.V.W.M. de Vries, Characterization of polymeric foams, Eindhoven University of

499   Technology, 2009.

500

501

502

503

504

505

506

507 **FIGURE CAPTIONS**

508

509 **Figure 1.** Raman spectra (a) and I_D/I_G ratio (b) of exfoliated graphene fractions and graphite.

510 **Figure 2.** AFM height images (left) and cross sectional profiles (right) of (a) S5, (b) S4, (c) S3 and

511 (d) S1 graphene fractions.

512 **Figure 3.** S1, S3, S4 and S5 dispersions prepared at 0.005 mg mL^{-1} in CH

513 **Figure 4.** TEM image of analyzed S1 graphene flake.

514 **Figure 5.** TEM images (a and b) taken from zone 1 and (c) taken from zone 2 defined in

515 previous figure (left), TEM images obtained from the areas indicated by the dashed rectangles on the

516 left (center) and TEM images obtained from the areas indicated by the dashed rectangles on the center

517 (right).

518 **Figure 6.** Intensity profiles calculated along the white lines shown in (a) Figure 5a right, (b) Figure

519 5b right, and (c) Figure 5c right.

520 **Figure 7.** EFM phase images obtained at bias voltage of -6 V (left), 0V (center) and 6 V (right) of

521 S1 graphene fraction. Scan size: 2 µm x 2 µm

522 **Figure 8.** SEM images of (a) foam matrix, (b) FG1 and (c) FG2 nanocomposites obtained at 50X

523 magnification and SEM images of (d) FG1 and (e) FG2 nanocomposites obtained at 10000X

524 magnification.

525 **Figure 9.** (a) Intensity-voltage curves of nanocomposites and (b) evolution of the electrical

526 resistance of nanocomposites with the deformation.

527